

X-ray iron line variability: constraints on the inner accretion disk

Christopher S. Reynolds

JILA, University of Colorado, Campus Box 440, Boulder, CO 80309

Abstract. After reviewing the basic physics of X-ray reflection in AGN, we present three case studies which illustrate the current state of X-ray reflection studies. For the low-luminosity AGN NGC 4258, we find that the iron line is much narrower than is typically found in higher luminosity AGN. We argue that this is evidence for either a truncated cold accretion disk (possibly due to a transition to an advection dominated accretion flow at $r \sim 100 GM/c^2$) or a large ($r \sim 100 GM/c^2$) X-ray emitting corona surrounding the accretion disk. We also present results for the higher luminosity Seyfert nuclei in NGC 5548 and MCG-6-30-15. In both of these sources, *RXTE* shows that the iron line equivalent width decreases with increasing luminosity. Furthermore, the iron line equivalent width is found to be *anticorrelated* with the relative strength of the reflection continuum, contrary to all simple reflection models. It is proposed that continuum-flux correlated changes in the ionization of the accretion disk surface can explain this spectral variability. Finally, we address the issue of X-ray iron line reverberation in the light of these complicating factors.

1. Introduction

AGN are observed to be copious X-ray emitters. These X-rays are thought to originate from the innermost regions of an accretion disk around a central supermassive black hole. Since the accretion disk itself is expected to be an optical/UV emitter, the most likely mechanism producing the X-rays is inverse Compton scattering of these soft photons in a hot and tenuous corona that sandwiches the accretion disk. Thus, in principle, the study of these X-rays should allow the immediate environment of the accreting black hole as well as the exotic physics, including strong-field general relativity, that operates in this environment to be probed.

In the past decade, X-ray astronomy has begun to fulfill that promise. Guided by observations with the *Ginga*, ASCA, RXTE and BeppoSAX satellites, there is a broad consensus that X-ray irradiation of the surface layers of the accretion disk in a class of AGN known as Seyfert 1 galaxies gives rise to fluorescent $K\alpha$ emission line of cold iron via the process of “X-ray reflection”. Accompanying the iron line is a reflected continuum possessing a characteristic shape that is determined by the competing effects of photoelectric absorption and Compton scattering.

In this contribution, I will review the basic physical processes leading to the observed X-ray reflection signatures, and the evidence leading us to believe that they do indeed originate from the innermost regions of the accretion disk. We will then discuss three recent observational campaigns on NGC 4258 (M106), NGC 5548 and MCG–6-30-15. The purpose of presenting results from these campaigns is to describe the successes, and mysteries, resulting from recent studies of X-ray reflection signatures.

2. X-ray reflection spectra and broad iron lines

The basic physics of X-ray ‘reflection’ can be understood by considering a hard X-ray (power-law) continuum illuminating a semi-infinite slab of cold gas. In this context, ‘cold’ is taken to mean that metal atoms are essentially neutral, but H and He are mostly ionized. When a hard X-ray photon enters the slab, it is subject to a number of possible interactions: Compton scattering by free or bound electrons, photoelectric absorption followed by fluorescent line emission, or photoelectric absorption followed by Auger de-excitation. A given incident photon is either destroyed by Auger de-excitation, scattered out of the slab, or reprocessed into a fluorescent line photon which escapes the slab.

Figure 1 shows the results of a Monte Carlo calculation which includes all of the above processes (Reynolds 1996; based on similar calculations by George & Fabian 1991). Due to the energy dependence of photoelectric absorption, incident soft X-rays are mostly absorbed, whereas hard photons are rarely absorbed and tend to Compton scatter back out of the slab. This gives the reflection spectrum a broad hump-like shape. In addition, there is an emission line spectrum resulting primarily from fluorescent $K\alpha$ lines of the most abundant metals. The iron $K\alpha$ line at 6.4 keV is the strongest of these lines.

For most geometries relevant to this discussion, the observer will see this reflection component superposed on the direct (power-law) primary continuum. Under such circumstances, the main observables of the reflection are a flattening of the spectrum above approximately 10 keV (as the reflection hump starts to emerge) and an iron line at 6.4 keV. For solar or cosmic abundances and a plane-parallel slab geometry, the expected equivalent width of the iron line is 150–200 eV (George & Fabian 1991; Reynolds, Fabian & Inoue 1995).

A major advance came with the launch of *ASCA* and its medium-resolution CCD spectrometers. A long (4.5 day) observation of the bright Seyfert galaxy MCG–6-30-15 in July-1994 allowed the iron line profile to be determined with some accuracy. The resulting line profile is shown in Fig. 2 (published by Tanaka et al. 1995). The line was found to be *extremely* broad (almost 10^5 km s $^{-1}$ FWZI) and asymmetric in so far that it possesses an extensive red-wing. Such a broad and asymmetric line is expected if the X-ray reflection is occurring in the inner regions of an accretion disk — strong line-of-sight Doppler shifts, transverse Doppler shifts and gravitational redshifts combine to produce an extensive low-energy wing and a sharp truncation of the line at high-energies (Fabian et al. 1989). Tanaka et al. (1995) showed that the MCG–6-30-15 data is in good agreement with the disk model provided the inclination of the disk is $\theta \approx 27^\circ$ and line fluorescence occurs down to $6GM/c^2$, the innermost stable orbit around a

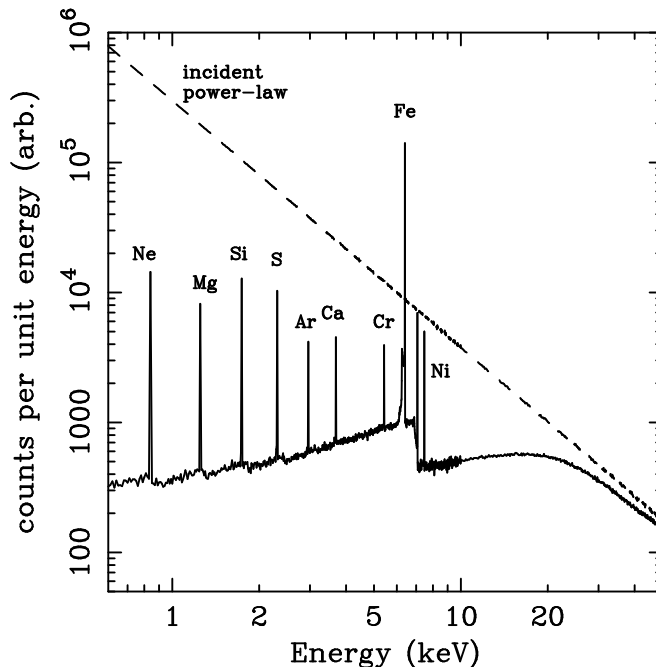


Figure 1. X-ray reflection from an illuminated slab. Dashed line shows the incident continuum and solid line shows the reflected spectrum (integrated over all angles). Monte Carlo simulation from Reynolds (1996).

Schwarzschild black hole. *This result is the best evidence to date for a radiatively-efficient accretion disk around a black hole in any object.*

Subsequent studies of large samples of objects by Nandra et al. (1997) confirmed the presence of these features in many other Seyfert 1 galaxies, and show that there is a tendency for the iron lines to indicate face-on accretion disks (as expected for Seyfert 1 nuclei from the unified Seyfert scheme).

3. Alternative models for broad iron lines

The claim that iron line studies are probing the region within a few gravitational radii of the black hole is a bold one, and should be tested against other models at every opportunity. Given the quality of data, the July-1994 MCG-6-30-15 line profile has become a test bed for such comparisons.

Fabian et al. (1995) examined many alternative models including lines from mildly relativistic outflows, the effect of absorption edges on the observed spectrum, and broadening of the line via comptonization. Fabian et al. found that none of these models were viable alternatives for the MCG-6-30-15 line profile. The idea of producing the broad line via Comptonization has been

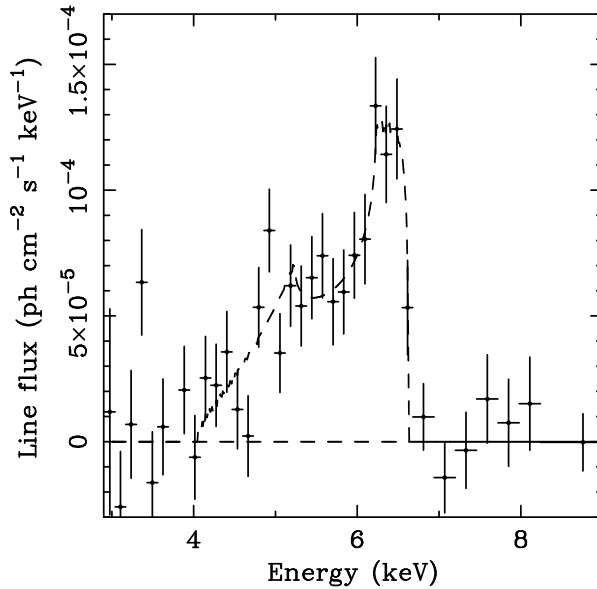


Figure 2. Iron line profile from the long 1994 *ASCA* observation of MCG-6-30-15. From Tanaka et al. (1995).

revived recently by Misra & Kembhavi (1997) and Misra & Sutaria (1999). They argue that the spectrum initially consists of a narrow iron line superposed on a power-law continuum and that Comptonization in a surrounding cloud with optical depth $\tau \sim 4$ produces the broad line. The Comptonizing cloud must be both cold ($kT < 0.5$ keV in order to predominately downscatter rather than upscatter the line photons), and fully-ionized (since no strong iron absorption edges are seen in the continuum spectrum). The cloud is kept fully ionized and yet cool by postulating that the continuum source has a very luminous optical/UV component.

There are strong arguments against such a model. Since the power-law continuum emission also passes through any such Comptonizing cloud, one would observe a break in the continuum spectrum at $E_{\text{br}} \sim m_e c^2 / \tau^2 \sim 30$ keV. Such a break is not observed in the *BeppoSAX* (Guainazzi et al. 1999) or *RXTE* data (Lee et al. 1999) for MCG-6-30-15 (see Misra 1999). Also, both continuum variability (which is seen on timescales as short as 100 s) and ionization arguments limit the size of the Comptonizing cloud in MCG-6-30-15 to $R < 10^{12}$ cm. The essence of this ionization argument is that the ionization parameter at the outer edge of the cloud (which, for a fixed cloud optical depth, scales with cloud size as $\xi \propto 1/R$) must be sufficiently high that all abundant metals, including iron, are fully ionized (Fabian et al. 1995; Reynolds & Wilms 2000). In the case of MCG-6-30-15, these constraints on the cloud size turn out to so tight that the postulated optical/UV component required to Compton cool the cloud would violate the black body limit (Reynolds & Wilms 2000). Comptonization

moreover provides a poor fit (Ruszkowski & Fabian 2000). Hence, we consider the Comptonization model for the broad iron line not to be viable.

In another alternative model, Skibo (1997) has proposed that energetic protons transform iron in the surface of the disk into chromium and lower Z metals via spallation which then enhances their fluorescent emission. With limited spectral resolution, such a line blend might appear as a broad skewed iron line. This model suffers both theoretical and observational difficulties. On the theoretical side, high-energy protons have to be produced and slam into the inner accretion disk with a very high efficiency (Skibo assumes $\eta = 0.1$ for this process alone). On the observational side, it should be noted that the broad line in MCG-6-30-15 (Tanaka et al 1995) is well resolved by the *ASCA* SIS (the instrumental resolution is about 150 eV at these energies) and it would be obvious if it were due to several separate and well-spaced lines spread over 2 keV.

4. Case study I — the low luminosity AGN NGC 4258

Low luminosity AGN (LLAGN) are almost certainly systems which are accreting at very low Eddington fractions. This places them in a regime of accretion which has been the subject of active theoretical work for many years. It was realized by several authors that when the accretion rate is low (relative to the Eddington rate), an accretion disk may switch into a hot, radiatively-inefficient mode (Ichimaru 1977; Rees 1982; Narayan & Yi 1994; Narayan & Yi 1995). In essence, the plasma becomes so tenuous that the timescale for energy transfer from the protons to the electrons (via Coulomb interactions) becomes longer than the inflow timescale. The energy remains as thermal energy in the protons (which are very poor radiators) and gets advected through the event horizon of the black hole. These are the so-called Advection Dominated Accretion Flows (ADAFs¹). ADAFs are to be contrasted with ‘standard’ radiatively-efficient accretion disks in which the disk remains cool and geometrically thin all of the way down to the black hole (Shakura & Sunyaev 1973; Novikov & Thorne 1974).

LLAGN provide an ideal laboratory in which to study ADAFs. If the central regions of LLAGN accretion disks are operating in an ADAF mode, we would not expect to observe broad iron lines since the ADAF is far too hot to contain combined iron ions. On the other hand, if we see broad iron lines from a LLAGN, this would be strong evidence for radiatively efficient disks even at these low accretion rates. However, the fact that LLAGN are faint has hampered such detailed X-ray studies of these sources.

In an attempt to study one LLAGN in some detail, we performed a 200 ksec joint *ASCA*/*RXTE* observation of the nearby LLAGN NGC 4258. A full discussion of this observation is presented in Reynolds, Nowak & Maloney (2000). Here, we summarize the iron line properties of this object.

¹In recent years there has been a large amount of work on advective accretion flows, with a corresponding expansion in terminology and acronyms (e.g. ADIOS, BDAF, and CDAF). See Prof. Narayan’s contribution in these proceedings for a fully discussion of the various types of advective accretion flow. Here, we use the term ADAF to encompass all such accretion flows which are radiatively inefficient.

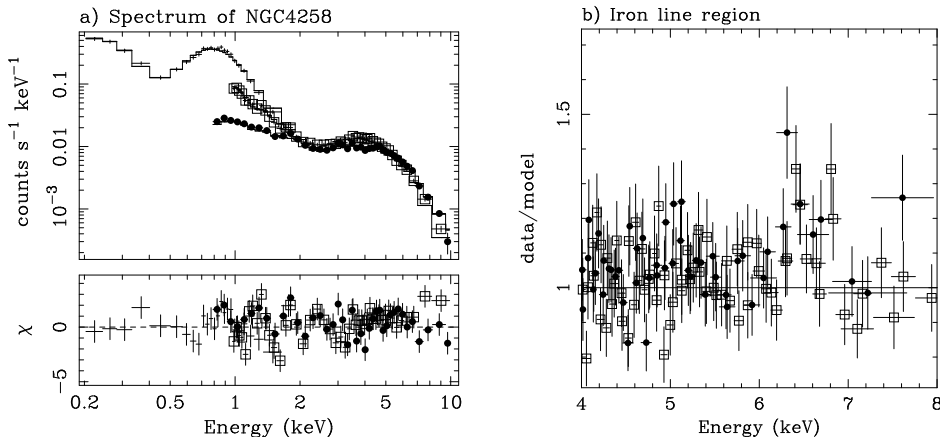


Figure 3. Panel (a) shows the joint *ROSAT*/*ASCA* spectrum for NGC 4258 fit with model-F from Table 1. The *ROSAT* data are the plain crosses. For clarity, only data from the SIS0 (open squares) and GIS2 (filled circles) instruments on board of *ASCA* are shown. Panel (b) shows iron line region of the spectrum with less severe binning, also referenced to model-F from Table 1. The presence of a fluorescent iron line is clear. These are both folded spectra (in the sense that they include the instrumental response).

As can be seen in Fig. 3, we clearly detect a iron line with an equivalent width of $W_{K\alpha} = 107^{+42}_{-37}$ eV and a velocity width of $< 22000 \text{ km s}^{-1}$ (FWHM) which is much narrower than those seen in higher luminosity Seyfert galaxies. If it is assumed that the observed iron line originates from the accretion disk, then we can use relativistic “disk-line” models to place constraints on the location of the line emission. Using such models it is found that the narrowness of the line implies that the bulk of the line emission originates from a distance $r > 100 GM/c^2$ from the black hole. Such a large line emitting radius is consistent with the ADAF model for NGC 4258 (Lasota et al. 1996) in which the thin fluorescing accretion disk goes through an transition into an ADAF at about $r \sim 100 GM/c^2$. However, the data are also consistent with a radiatively efficient fluorescing disk extending down to the radius of marginal stability and a large ($r \sim 100 GM/c^2$) X-ray corona. In this latter case, there would be faint broad wings to the line profile which could be found with a high signal-to-noise *XMM-Newton* spectrum. One way or another, the iron line properties of this LLAGN are different to those of many higher-luminosity Seyfert galaxies which display a broad iron line indicating radiative disks and small ($\sim 10 GM/c^2$) X-ray emitting regions.

We cannot rule out the possibility that most (or all) of the observed iron line originates from matter that is not associated with the accretion disk. However, simple arguments lead us to disfavor such a scenario. Consider iron line emission in a geometrically-thick torus surrounding the accretion disk of NGC 4258. An upper limit to the column density of this structure along our line of sight to the AGN is given by the observed column density of $N_H \approx 10^{23} \text{ cm}^{-2}$. If we suppose that this torus is in the same plane as the accretion disk (so that we are

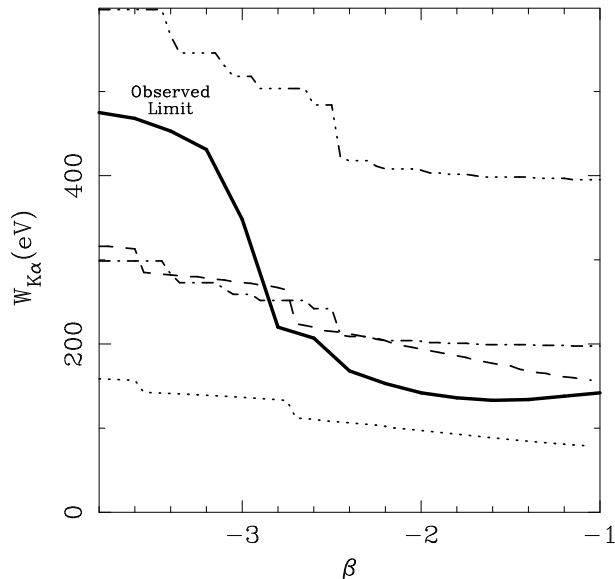


Figure 4. Constraints on the presence of a “Seyfert-like” iron line in the case where the observed narrow line is modeled by a separate narrow Gaussian component. The broad line is modeled as originating in an accretion disk around a Schwarzschild black hole, with a disk inclination of $i = 85^\circ$ and an inner line emitting radius of $r_{\text{br}} = 6GM/c^2$. The solid line shows the upper limit on the equivalent widths as a function of the emissivity index β . The dotted and dashed lines show the theoretical expectation, taking into account limb-darkening and light bending effects, assuming that the iron line has an equivalent width of 200 eV and 400 eV, respectively, when the disk is viewed face on. The dot-dashed and dot-dot-dot-dashed lines show the theoretical expectation when limb-darkening is absent (see text) assuming that the iron line has an equivalent width of 200 eV and 400 eV, respectively, when the disk is viewed face on.

also viewing it edge-on), it is plausible to assume that we are looking through the optically-thickest part of the torus. We can then show that the maximum equivalent width produced by fluorescence of this material is $W_{\text{Fe,max}} \approx 65 \text{ eV}$ (Reynolds, Nowak & Maloney 2000). However, there are several reasons why this upper limit would almost certainly not be achieved. Firstly, modeling of the accretion disk warp strongly suggests that our line of sight intercepts the disk and that the bulk of the column density which obscures the AGN originates in the disk (Herrnstein, priv. communication). Therefore, we might expect significantly smaller column densities along lines of sight that have smaller inclinations angles relative to the accretion disk. Secondly, the accretion disk may well occult half of this fluorescing cloud, thereby reducing this prediction further. Thus, the true iron line from surrounding non-disk material may well be reduced from our naive prediction by a factor of several.

Despite these arguments, let us now suppose that the observed iron line is *not* associated with the accretion disk. Our data then permit the presence of a “Seyfert-like” broad iron line which is buried in the noisy continuum data. If we suppose NGC 4258 to possess a normal “Seyfert-like” broad iron line (with an intrinsic equivalent width in the range 200–400 eV, modified by the light bending and limb-darkening effects that are important in edge-on systems such as NGC 4258), we can set some interesting constraints (see Fig. 4). In particular, we can rule out models in which the limb-darkening is very weak (as would be the case if, for example, the $\tau_e = 1$ surface of the accretion disk is very filamentary rather than planar). Of course, higher signal-to-noise data from *XMM-Newton* are required if one is to constrain the nature of the disk in this object any further.

5. Case study II — an EUV/X-ray campaign on NGC 5548

In the rest of this contribution, we turn to the properties of higher luminosity systems. Firstly, we shall discuss the classical Seyfert galaxy NGC 5548.

We² observed NGC 5548 with *EUVE*, *ASCA*, and *RXTE* in June/July 1998. The main part of the campaign consisted of four observations (with all of these satellites simultaneously) separated by approximately one week. One of these observations (18-June-1998) was substantially longer than the others (~ 110 ksec of good data, as compared with an average of ~ 30 ksec for the other observations). This long observation provided us with intensive monitoring over a period of 3 days from the EUV to hard X-rays. The various aspects of this campaign are discussed in detail in Chiang et al. (2000).

Although not strictly related to X-ray reflection studies, it is worth mentioning the continuum variability properties found during this campaign. Figure 5 shows the *EUVE*, *ASCA* and *RXTE* light curves for our long observation. The most distinct feature is a step at $\sim 2 \times 10^4$ s. By computing the z-transformed discrete correlation function (ZDCF; Alexander 1997) between these various data, we find clear evidence that the EUV emission leads the *RXTE*-band emission by ~ 30 ksec, and the *ASCA*-band emission by ~ 15 ksec. If confirmed, this results has at least two important implications. Firstly, the EUV emission cannot simply be reprocessed hard X-ray emission since these scenario would predict the EUV to lag the hard X-rays. Secondly, if we make the assumption that the observed lags are due to the Compton upscattering of seed photons, we can constrain the size of the Comptonizing region to be about $10 GM/c^2$ for a $10^8 M_\odot$ black hole.

Returning to the issue of X-ray reflection, this campaign produced a major surprise. Before discussing the data, it is worth recapping our theoretical expectations from simple X-ray reflection models. For a fixed disk/corona geometry and ionization state, we expect the iron line equivalent width to remain constant provided one is probing timescales longer than the reverberation timescale of the system (which is always the case for spectral studies with *ASCA* and *RXTE*).

²The team of investigators consisted of Omer Blaes (UCSB), James Chiang (Colorado), Greg Madjeski (NASA-GSFC), Pawel Magdziarz (deceased), Hermann Marshall (MIT-CSR), Mike Nowak (Colorado) and myself.

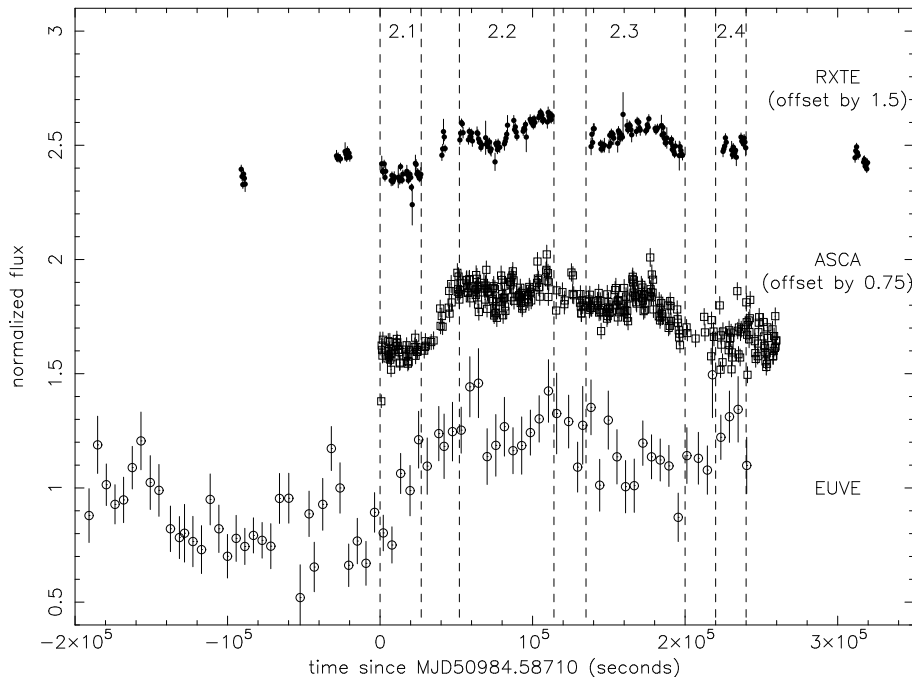


Figure 5. *EUVE*, *ASCA*-SIS, and *RXTE*-PCA light curves for the long observation of NGC 5548. All light curves have been normalized to a unity mean level. For clarity, the *ASCA* and *RXTE* light curves have then been offset by 0.75 and 1.5, respectively.

If the iron line equivalent width does change due to, for example, a change in the geometry of the system, then the relative strength of the reflection continuum would be expected to vary in step. In other words, we expect a strict proportionality between the iron line equivalent width and relative strength of the reflection continuum.

Figure 6 shows the various spectral parameters, measured from the *RXTE* data, for NGC 5548 as a function of the 2–10 keV continuum flux of the source. We found that the equivalent width of the iron line declined as the continuum source flux increased — in fact, the iron line *flux* was consistent with being constant. Simultaneous spectroscopy with *ASCA* showed the iron line to be broadened. Hence, the line does appear to be originating from the central regions ($r < 50 GM/c^2$) of the accretion disk and, for any reasonable size black hole mass, the constancy of the line flux cannot be due to light travel time effects. Moreover, the relative reflection fraction (R) fails to track the changes in the iron line equivalent width. Indeed, these quantities appear to be weakly *anti-correlated* (see Fig. 7), contrary to the simple reflection models.

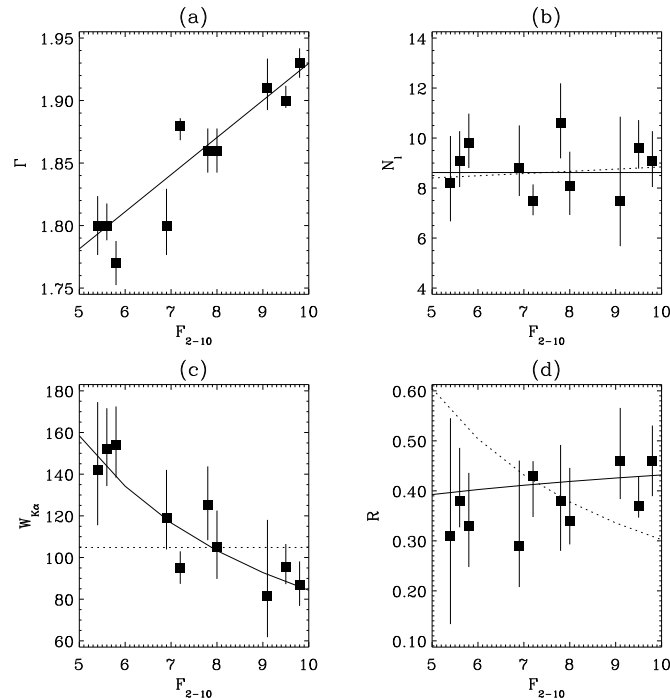


Figure 6. *RXTE* results on NGC 5548. Panel (a) shows the well-known trend for the X-ray photon index to increase slightly as the continuum flux increases (possibly due to Compton cooling of the corona). Panels (b) and (c) show that the iron line possesses approximately constant flux (the dotted line in panel-c shows the best fitting constant). Panel (d) shows that the relative strength of the reflection continuum is approximately constant or slightly increasing. The dotted line shows the predicted strength of the reflection continuum assuming that it tracks the iron line equivalent width. Figure from Chiang et al. (2000).

6. Case study III — the X-ray campaign on MCG–6-30-15

A very long, simultaneous *ASCA*/*RXTE* observation of the Seyfert 1 galaxy MCG–6-30-15 by an (almost) independent team of researchers³ revealed very similar spectral results to those obtained for NGC 5548. Figure 8 shows the clear anti-correlation between iron line equivalent width and the relative strength of the reflection continuum found by Lee et al. (2000). To produce this figure, almost nine days of *RXTE* data have been binned into four flux-sorted spectra. Unlike with NGC 5548, these data strongly require a change in the relative strength of the reflection continuum as well as the iron line equivalent width. The details of this observation are discussed by Lee et al. (1999, 2000).

³The team of investigators consisted of Niel Brandt (PSU), Andy Fabian (Cambridge), Kazushi Iwasawa (Cambridge), Julia Lee (MIT) and myself.

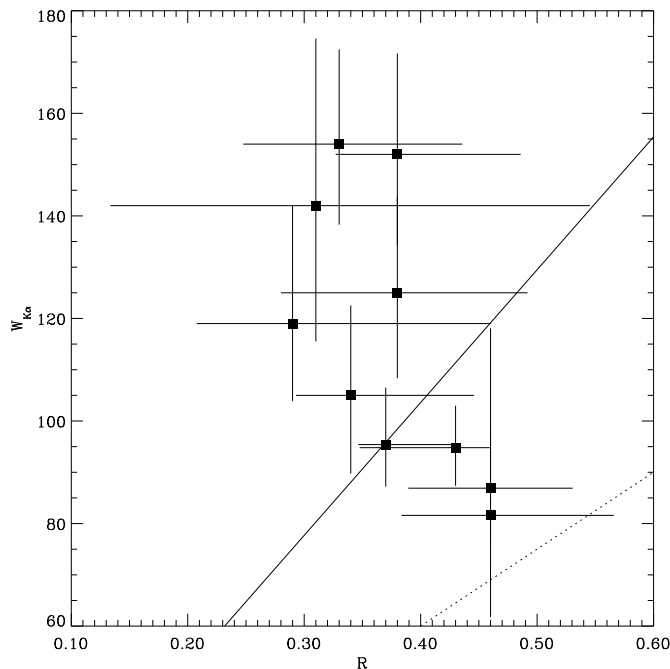


Figure 7. Iron line equivalent width $W_{K\alpha}$ vs. the relative strength of the reflection continuum \mathcal{R} for NGC 5548. The dotted line is the expected linear relationship assuming solar abundances for the cold reflector (George & Fabian 1991). The solid line is the best fit proportionality relationship which is still in conflict with the data at the 89% level. Figure from Chiang et al. (2000).

This particular *RXTE* campaign yielded data of an almost unprecedented nature — the observation lasted over 100 consecutive orbits of *RXTE*, giving us dense coverage ($> 50\%$) for almost 9 days. Reynolds (2000) took advantage of this unique dataset and performed a detailed search for delays between a continuum band (2–4 keV) and the iron line band (5–7 keV) in an attempt to search for iron line reverberation effects. In essence, the method of Press, Rybicki & Hewitt (1992) was used to interpolate across the gaps in the continuum light curve (caused primarily by Earth occultation) and estimate the errors in the interpolation. Figure 9a shows a small portion of the light curve, together with the Press et al. (1992) reconstruction. The continuous (interpolated) continuum light curve can then be folded through a trial transfer function and compared with the line-band light curve in a χ^2 sense (e.g., Fig. 9b shows the χ^2 surface that results from such a procedure). By varying the parameters of the trial transfer function, we can place constraints on any time delays between bands. No time delays were found on timescales down to 500–1000 s. Instead, it was found that the line flux remained constant, thereby extending the result of Lee et al. (2000) down to these timescales.

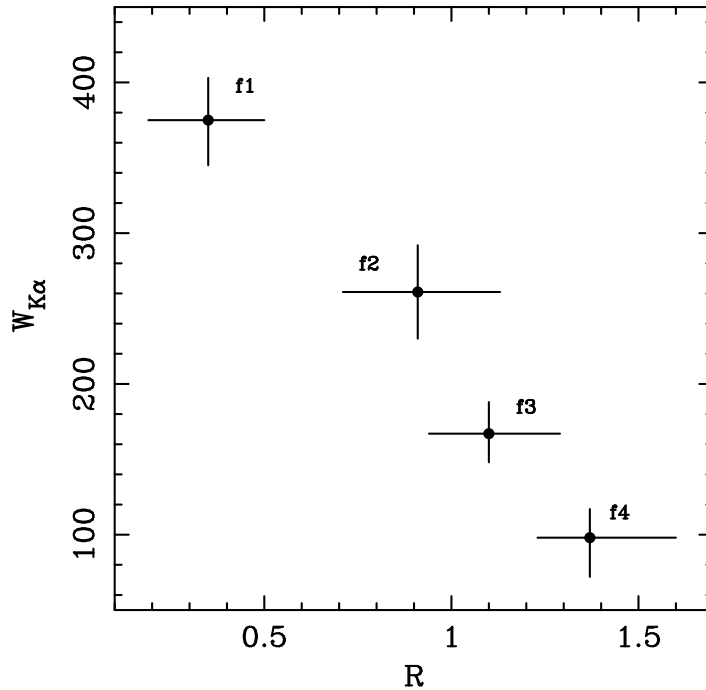


Figure 8. Iron line equivalent width $W_{K\alpha}$ vs. the relative strength of the reflection continuum R for MCG–6-30-15. Flux states f1–f4 are in order of increasing continuum flux. Figure from Lee et al. (2000).

7. Evidence for flux-correlated changes in the disk’s ionization

To summarize the mysteries resulting from the NGC 5548 and MCG–6-30-15 campaigns, it is found that:

1. The iron line *flux*, rather than the equivalent width, appears to remain approximately constant as the continuum X-ray source undergoes rapid variability. In NGC 5548, this result is derived by direct X-ray spectral fitting and so applies on timescales of ~ 50 ksec (which is approximately timescale that can be probed via such methods). In MCG–6-30-15, the spectral fitting of Lee et al. (2000) combined with the analysis of Reynolds (2000) leads us to believe that such behavior occurs on all timescale from 500 ksec down to 500 s. This cannot be due to light travel delays.
2. The iron line equivalent width and relative strength of the reflection continuum are *anti-correlated*, in contradiction to simple X-ray reflection models.

Changing the ionization state of the surface of the accretion disk is one of the few ways of breaking the expected proportionality between the iron line equivalent and the (inferred) relative strength of the reflection continuum.

Reynolds (2000) proposed a toy model to explain these *RXTE* results (Fig. 10). In this model, there is a radial ionization gradient on the disk surface due to the radial dependence of both the ionizing flux and the density of the surface

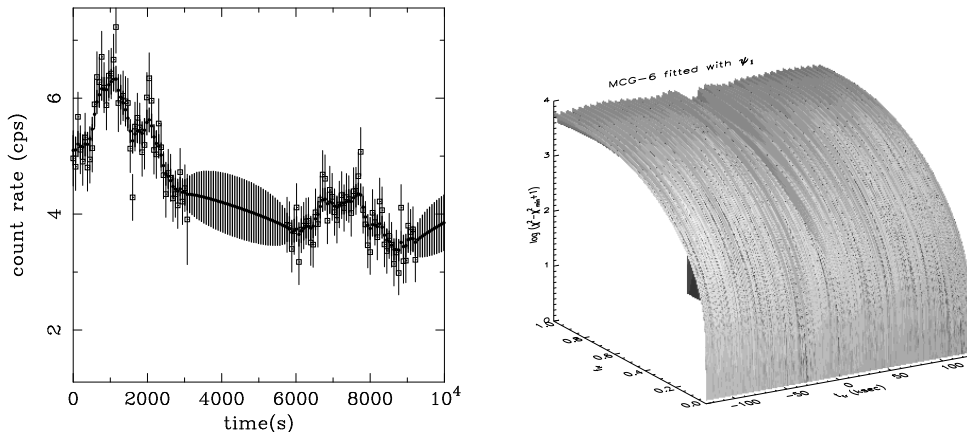


Figure 9. Panel (a) shows 2 orbits of the 2-4 keV light curve (open squares and thin error bars) together with the reconstructed light curve (filled circles and heavy error bars). Panel (b) shows the χ^2 surfaces and confidence contours resulting from applying trial transfer function $\psi_1 = (1 - f_{\text{tr}})\delta(t) + f_{\text{tr}}\delta(t - t_{\text{tr}})$ to the reconstructed continuum light curves and comparing with the line band light curve. The surface is plotted using $\log_{10}(\chi^2 - \chi_{\text{min}}^2 + 1)$ as the ordinate in order to display the topography of the region near the minimum. The χ^2 minimum is along the line $f_{\text{tr}} = 0$ indicating that no time lag has been detected. Figure from Reynolds (2000).

layers. The surface of the inner disk, which is strongly irradiated by the primary X-ray flux, is highly ionized and acts as a pure Compton mirror. It thereby fails to imprint distinct (atomic) features in the observable spectrum. By contrast, the outer disk surface (starting at $\sim 20 - 50 GM/c^2$) possesses a relatively low ionization parameter and produces ‘neutral-like’ X-ray reflection signatures such as those calculated by George & Fabian (1991). The interesting and uncertain processes occur in the partially ionized intermediate zone of the accretion disk. In this region, there are two possible physical mechanisms by which the iron line can be strongly suppressed relative to the reflected continuum. These mechanisms are described in the next two paragraphs. Reynolds (2000) noted that, if the boundaries between these zones are defined by some given set of ionization parameters, the zones will move as the primary continuum flux varies. If the primary continuum flux increases, the fluorescing outer zone will move outwards and so subtends a smaller solid angle as seen by the primary X-ray source. The observed iron line equivalent width will then be seen to decrease. However, the measured relative strength of the reflection continuum may remain roughly constant if the intermediate zone still produces bound-free absorption features in the reflection continuum.

As mentioned above, there are at least two mechanisms which may operate in the intermediately ionized zone of the accretion disk to suppress iron line emission relative to the reflection continuum. Nayakshin, Kazanas & Kallman (2000) showed that the well-known thermal instability of photoionized plasma could lead to the formation of a highly ionized skin on the surface of the accretion



Figure 10. The toy model of an ionized accretion disk that may produce the observed spectral variability. The inner (light) region is strongly irradiated, highly ionized and does not produce any observable reflection features. The outer (dark) region is weakly irradiated, weakly ionized, and produces ‘neutral-like’ reflection signatures. The partially ionized middle zone may be able to produce a significant reflection continuum with very little iron line (see text). As the primary X-ray source varies in intensity, the boundaries between these zones (presumably defined by some given ionization parameters) will move, thereby changing the relative strengths of the iron line and reflection continuum. See Reynolds (2000) for a more detailed discussion.

disk. Compton scattering in this skin would smear out sharp spectral features such as the iron line, possibly to the level where line photons from this region would no longer be identified with the iron line. However, very broad spectral features such as the iron edge and broad hump that observationally define the reflection continuum, would be much less affected by Compton scattering in the skin. Thus, from the observational point of view, the presence of such a skin might reduce the iron line strength while leaving the strength of the reflection continuum unaffected.

The second line destruction mechanism is that of resonant trapping followed by Auger destruction (Ross & Fabian 1993). A fluorescent iron line photon is typically created at an optical depth of $\tau_e \sim 1$. However, when the bulk of the ions are at least as ionized as Fe XVII, the presence of a vacancy in the L-shell of the iron ions leads to resonant scattering of the line photons with a rather small path length. If, furthermore, the bulk of the ions possess at least two L-shell electrons (i.e. Fe XXIII or less), then the Auger effect acts as a photon destruction mechanism. The combination of resonant ‘trapping’ and Auger ‘destruction’ might reduce the observed iron line to a very small strength.

Clearly, more work is needed on the physics and modeling of ionization accretion disks in order to assess whether such a toy model can explain the mysterious X-ray variability that we see in current *RXTE* data.

8. Down to the reverberation timescale

The rapid X-ray variability of many Seyfert galaxies leads us to believe that the primary X-rays are emitted during dramatic flare-like events in the accretion disk corona. When a new flare becomes active, the hard X-rays from the flare will propagate down to the cold disk and excite iron fluorescence. Due to the finite speed of light, the illumination from the flare sweeps across the disk, and the reflected X-rays act as an ‘echo’ of this flare. Such flaring will cause temporal changes in the iron line profile and strength due to the changing illumination pattern of the disk and, more interestingly, time delays between the observed flare and the its fluorescent echo. This latter effect is directly analogous to the

optical broad line reverberation that is a major theme of this meeting. The observational study of iron line reverberation is beyond the capabilities of current instruments (even, probably, *XMM-Newton*) but should be within reach of future high-throughput X-ray observatories such as *Constellation-X* and *XEUS*.

In recent work, it has been shown that interesting diagnostics of the black hole spin and X-ray source geometry are encoded within the iron line reverberation pattern (Reynolds et al. 1999; Young & Reynolds 2000; Ruzsowski 2000). However, there are many complications and issues that will affect our ability to extract these reverberation signatures from real data. Firstly, there are likely to be several X-ray flares active at any one time which will give overlapping reverberation signatures. Moreover, due to the fact that the X-ray emitting corona is probably extended on the same spatial scales as the inner disk, each X-ray emitting flare will have its own distinct transfer function. This breaks the linearity of the transfer problem. Young & Reynolds (2000) showed that if there are only a small number of powerful flares, the individual transfer functions can be identified and separated in *Constellation-X* data. However, we must examine more powerful statistical methods for extracting useful information from this system.

Possible reverberation signatures will be affected by short timescale ionization changes. The models of Reynolds et al. (1999) and Young & Reynolds (2000) assume that the disk has a fixed, fairly cold, ionization structure. However, as discussed extensively above, *RXTE* argues for ionization changes in the disk surface that are correlated with the continuum flux. On a local scale, this effect may be driven by ionization fronts that sweep across the disk when an X-ray flare erupts. In future work, these effects must be assessed so that instruments and observing strategies can be planned to study reverberation effects. It must be noted that, even though *RXTE* data argue for almost constant iron line flux due to the ionization changes, we would still expect to see variability of the line strength and/or profile on either the recombination timescale in the disk surface or the light-crossing timescale from the flare to the disk, whichever is longest.

Given all of these complications and difficulties, why bother to pursue the idea of iron line reverberation? The answer to this question is straightforward — until we have the technology to directly image the immediate environment of a black hole (and this is at least 20 years away), X-ray iron line reverberation is simply our best hope of mapping out the detailed astrophysical environment of supermassive black holes, including the effects of the black hole's spin.

9. Conclusions

In this contribution, we present three case studies in order to describe the current state of X-ray reflection studies in AGN. For the low-luminosity AGN NGC 4258, we find that the iron line is much narrower than is typically found in higher luminosity AGN. We argue that this is evidence for either a truncated cold accretion disk (possibly due to a transition to an ADAF at $r \sim 100 GM/c^2$) or a large ($r \sim 100 GM/c^2$) X-ray emitting corona surrounding the accretion disk. We also present results for the higher luminosity Seyfert nuclei in NGC 5548

and MCG–6-30-15. In both of these sources, *RXTE* shows that the iron line equivalent width decreases with increasing luminosity. Furthermore, the iron line equivalent width is found to be *anticorrelated* with the relative strength of the reflection continuum, contrary to all simple reflection models. It is proposed that continuum-flux correlated changes in the ionization of the accretion disk surface can explain this spectral variability. Finally, we address the issue of X-ray iron line reverberation in the light of these complicating factors.

10. Acknowledgements

The author appreciates support from Hubble Fellowship grant HF-01113.01-98A. This grant was awarded by the Space Telescope Institute, which is operated by the Association of Universities for Research in Astronomy, Inc., for NASA under contract NAS 5-26555. He also appreciates support from NASA under LTSA grant NAG5-6337, and the National Science Foundation under grants AST-9529170 and AST-9876887.

References

- Alexander T., 1997, in *Astronomical Time Series*, ed. D. Maoz et al., (Dordrecht: Kluwer), 163
- Chiang J. et al., 2000, *ApJ*, 528, 292
- Fabian A. C., Rees M. J., Stellar L., White N. E., 1989, *MNRAS*, 238, 729
- Fabian A. C. et al. 1995, *MNRAS*, 277, L11
- George I. M., Fabian A. C., 1991, *MNRAS*, 249, 352
- Guainazzi M. et al., 1999, *A&A*, 341, L27
- Ichimaru S., 1977, *ApJ*, 214, 840
- Lasota J.-P., Abramowicz M. A., Chen X., Krolik J., Narayan R. 1996, *ApJ*, 462, 142
- Lee J., Fabian A. C., Reynolds C. S., Brandt W. N., Iwasawa K., 2000, *MNRAS*, in press
- Lee J., Fabian A. C., Brandt W. N., Reynolds C. S., Iwasawa K., 1999, *MNRAS*, 310, 973
- Misra R., 1999, IUCAA preprint 32/99
- Misra R., Kembhavi A. K., 1998, *ApJ*, 499, 205
- Misra R., Sutarra F. K., 1999, *ApJ*, 517, 661
- Nandra K., George I. M., Mushotzky R. F., Turner T. J., Yaqoob T., 1997, *ApJ*, 477, 602
- Nayakshin S., Kazanas D., Kallman T. R., 2000, *ApJ*, submitted (astro-ph/9909359)
- Narayan R., Yi I., 1995, *ApJ*, 452, 710
- Narayan R., Yi I., 1994, *ApJ*, 428, L13
- Novikov I. D., Thorne K. S., 1973, in *Black Holes*, eds C. DeWitte & B. S. DeWitte (Gordon and Breach Science Publicaters, New York), P.344
- Press W. H., Rybicki G. B., Hewitt J. N., 1992, *ApJ*, 385, 404

- Rees M. J., 1982, in Riegler G., Blandford R. D., eds, *The Galactic Center*, Am. Inst. Phys., New York, p.166.
- Reynolds C. S., 1996, PhD thesis, University of Cambridge
- Reynolds C. S., 2000, *ApJ*, 533, 811
- Reynolds C. S., Wilms J., 2000, *ApJ*, 533, 821
- Reynolds C. S., Fabian A. C., Inoue H., 1995, *MNRAS*, 276, 1311
- Reynolds C. S., Nowak M. A., Maloney P. R., 2000, *ApJ*, in press (astro-ph/0004068)
- Reynolds C. S., Young A. J., Begelman M. C., Fabian A. C., 1999, *ApJ*, 514, 164
- Ross R. R., Fabian A. C., 1993, *MNRAS*, 261, 74
- Ruszkowski M., 2000, *MNRAS*, 315, 1
- Ruszkowski M., Fabian A. C., 2000, *MNRAS*, submitted
- Shakura N. L., Sunyaev R. A., 1973, *A&A*, 24, 337
- Skibo, J.G., 1997, *ApJ*, 478, 522
- Tanaka Y. et al., 1995, *Nat*, 375, 659
- Young A. J., Reynolds C. S., 2000, *ApJ*, 529, 101